Translational Oncology 67 (2026) 102738

Contents lists available at ScienceDirect

Translational Oncology

journal homepage: www.elsevier.com/locate/tranon

Integrated single-cell and bulk transcriptomics reveals STAB1 as a novel therapeutic target for ovarian cancer

Yuqiang Zhang [a,b,†], Juan Chen [a,b,†], Li Tang [a,b], Xiaohai Sun [a,b], Ling Yang [a,b,*], Zhaomei Zhong [a,b,*]

[a] Bao'an Clinical Institute of Shantou University Medical College, Guangdong Shenzhen 518000 China
[b] Shenzhen Bao'an Shiyan People's Hospital, Guangdong, Shenzhen 518000, China

ARTICLE INFO

Keywords:
Ovarian cancer
Single-cell RNA sequencing
Tumor microenvironment
STAB1
M2 Macrophage polarization

ABSTRACT

The immunosuppressive tumor microenvironment (TME) and intrinsic heterogeneity of ovarian cancer (OC) are primary drivers of therapeutic resistance and mortality. To deconvolute these complex dynamics and identify robust therapeutic targets, this study employed an integrative strategy combining ensemble machine learning algorithms with high-resolution single-cell transcriptomics and experimental validation. Through dual-feature selection (LASSO and SVM-RFE) applied to multi-cohort bulk transcriptomic data, we identified Stabilin-1 (STAB1) as a top-ranked prognostic determinant. Crucially, single-cell analysis of the OC ecosystem redefined the cellular localization of STAB1, revealing its predominant enrichment in LYVE1+ perivascular-like M2 macrophages and a hyper-aggressive, EMT-active tumor subpopulation. Validating these in silico insights, in vitro loss-of-function assays confirmed that STAB1 silencing in OC cell lines (A2780 and SK-OV-3) significantly suppressed cell proliferation, colony formation, and invasion. Collectively, our findings support STAB1 as a pivotal "dual-checkpoint" molecule that bridges the immunosuppressive stroma and the malignant epithelium, highlighting its potential as a novel therapeutic target for dismantling the ovarian cancer ecosystem.

Introduction

Ovarian cancer (OC) remains the most lethal gynecological malignancy worldwide, characterized by a deceptive asymptomatic progression that frequently leads to diagnosis at advanced metastatic stages [1]. Despite initial responsiveness to cytoreductive surgery and platinum-based chemotherapy, approximately 80 % of patients with advanced-stage disease experience recurrence due to the emergence of intrinsic or acquired chemoresistance, resulting in a 5-year survival rate of <45 % [2]. Recent genomic landscapes have highlighted that OC progression is driven not only by genetic aberrations in tumor cells but also by the dynamic and immunosuppressive tumor microenvironment (TME) [3]. Therefore, decoding the intricate crosstalk between malignant cells and their supportive niche is imperative for identifying robust therapeutic targets that can disrupt this pro-tumorigenic symbiosis.

Within the complex ecosystem of the OC TME, tumor-associated macrophages (TAMs) constitute the dominant immune population [4]. In response to microenvironmental cues, TAMs frequently polarize towards an alternatively activated M2 phenotype, which facilitates angiogenesis, suppresses anti-tumor immunity, and remodels the extracellular matrix (ECM) to support metastasis [5]. While traditional bulk transcriptomic analyses have identified numerous prognosis-related genes, these methods average gene expression across complex tissues, often obscuring the precise cellular source of these molecules—whether they originate from malignant epithelial cells or infiltrating stromal components [6]. The advent of single-cell RNA sequencing (scRNA-seq) has revolutionized this field, providing unprecedented resolution to map ligand-receptor interactions and virtually reconstruct the spatial signaling networks driving malignancy [7]. In parallel, the integration of Artificial Intelligence (AI) and Machine Learning (ML) with multi-omics data has emerged as a powerful strategy to accelerate target discovery, filtering out noise from high-dimensional datasets to pinpoint robust biomarkers [8]. However, a critical gap remains between computational predictions (*in silico*) and biological mechanisms (*in vitro/vivo*). Specifically, many predicted targets lack rigorous validation of their specific roles in orchestrating the interplay

* Corresponding authors at: Shenzhen Bao'an Shiyan People's Hospital, Guangdong, Shenzhen 518000, China.
E-mail addresses: YL567123@163.com (L. Yang), zmz518000@163.com (Z. Zhong).
† Equal authors.

https://doi.org/10.1016/j.tranon.2026.102738
Received 15 January 2026; Received in revised form 20 February 2026; Accepted 13 March 2026

between the immune stroma and cancer cells.

In this study, we employed a comprehensive "Bedside-to-Bench" strategy combining ensemble machine learning algorithms, high-resolution scRNA-seq, and experimental pharmacology. We initially identified Stabilin-1 (STAB1), a scavenger receptor typically associated with tissue homeostasis [9], as a top-ranked prognostic determinant in OC via LASSO and SVM-RFE algorithms. Crucially, utilizing single-cell analysis, we redefined the cellular localization of STAB1, revealing its predominant enrichment in perivascular-like M2 macrophages rather than tumor cells alone. Furthermore, computational inference of intercellular communication suggested a potential paracrine signaling network, predicting that STAB1-enriched macrophages might interact with tumor cells via ligand-receptor pairs such as the SPP1-CD44 axis. This provides a putative molecular basis for the observed Epithelial-Mesenchymal Transition (EMT) and stemness traits [10,11]. Finally, we experimentally validated that silencing STAB1 significantly impairs OC cell proliferation and invasion, confirming its potential as a therapeutic target that bridges the "malignant seed" and the "corrupt soil."

Methods

Data acquisition and preprocessing

Three independent Gene Expression Omnibus (GEO) datasets were retrieved from the NCBI GEO database: GSE65857 (32 ovarian cancer [OC] tumor samples vs. 32 matched normal tissues), GSE18520 (53 OC samples vs. 10 normal ovarian surface epithelia), and GSE14407 (12 papillary serous OC epithelia vs. 12 healthy ovarian surface epithelia). Raw microarray data were downloaded in CEL format and preprocessed using the affy package in R (version 4.3.0). Background correction, normalization, and probe summarization were performed with the Robust Multi-array Average (RMA) algorithm. For survival analysis and prognostic modeling, RNA-sequencing data and clinical information from The Cancer Genome Atlas Ovarian Cancer (TCGA OV) cohort ($n = 379$) were obtained from the UCSC Xena platform. Gene expression values were $\log_2$-transformed and normalized using the DESeq2 package. Probes mapping to multiple genes were removed, and the median value was selected for genes with multiple probes. For single-cell analysis, the high-resolution single-cell RNA sequencing (scRNA-seq) dataset GSE184880 was downloaded from the GEO database to map the cellular landscape of the OC tumor microenvironment (TME).

Differential gene expression analysis

Differentially expressed genes (DEGs) between OC tumor and normal samples were identified using the limma package in R. Linear models were fitted to the normalized expression data, and empirical Bayes moderation was applied to compute moderated t-statistics. DEGs were defined by $|\log_2 (\text{fold change})| > 1$ and adjusted P-value < 0.05 (Benjamini-Hochberg correction). Volcano plots were generated using the EnhancedVolcano package to visualize DEGs. Common DEGs across datasets were identified using Venn diagrams via the VennDiagram package. Heatmaps of the top 25 up- and downregulated DEGs were created with the pheatmap package, employing Euclidean distance and complete linkage clustering.

Feature selection for prognostic modeling

Feature selection was conducted using Least Absolute Shrinkage and Selection Operator (LASSO) regression via the glmnet package and Support Vector Machine Recursive Feature Elimination (SVM-RFE) via the e1071 package in R. For LASSO, 10-fold cross-validation was applied to select the optimal λ minimizing binomial deviance. For SVM-RFE, features were recursively eliminated based on their contribution to model accuracy, with performance evaluated by error rate and accuracy curves. Feature importance scores were derived from SVM coefficients. Overlaps between methods were visualized using Venn diagrams.

Construction and validation of a multi-gene prognostic signature

Univariate and multivariate Cox proportional hazards regression were performed using the survival package in R to identify independent prognostic factors ($P < 0.05$). A multi-gene risk signature was constructed based on regression coefficients. A nomogram integrating signature genes was built with the rms package for predicting 1-, 3-, and 5-year OS. Model calibration was assessed using calibration plots with 1000 bootstrap resamples and the Hosmer-Lemeshow test. Discriminatory performance was evaluated by receiver operating characteristic (ROC) curves and area under the curve (AUC) values using the pROC package in independent GEO validation datasets (GSE14407, GSE65857, GSE18520, GSE38666).

Single-cell RNA sequencing

Data Processing and Annotation Single-cell RNA-seq data were processed using the Seurat R package (version 4.3.0). Quality control strictly excluded cells with fewer than 200 or >6000 detected genes, or those containing greater than 20 % mitochondrial transcripts. Following normalization via the Log Normalize method, the top 2000 highly variable genes were identified for Principal Component Analysis (PCA). Unsupervised clustering was performed using the Find Neighbors and Find Clusters functions (resolution 0.5), and cell clusters were visualized using Uniform Manifold Approximation and Projection (UMAP). Cell lineages were annotated based on the expression of canonical markers, including EPCAM/KRT8 (Epithelial), CD68/C1QA (Macrophages), PECAM1 (Endothelial), COL1A1 (Fibroblasts), and lineage-specific lymphocyte markers.

Sub-clustering and phenotypic characterization

To interrogate cellular heterogeneity, macrophage and epithelial populations were subsetted for re-clustering and downstream analysis. Macrophage subpopulations were defined using functional markers such as LYVE1, CD163, and FCN1, and Spearman correlation analysis was employed to assess the association between STAB1 expression and M2 polarization signatures. Concurrently, epithelial tumor cells were stratified into STAB1-high and STAB1-low groups based on median expression levels. Differentially expressed genes (DEGs) were identified using the Wilcoxon rank-sum test to elucidate molecular phenotypes associated with epithelial-mesenchymal transition (EMT) and stemness.

Intercellular communication network analysis

Intercellular communication networks were constructed using the CellChat R package, utilizing the CellChatDB.human database as a reference. Global signaling patterns were characterized by computing communication probabilities and aggregated interaction weights to compare network density between normal and tumor tissues. Network centrality measures, specifically out-degree and in-degree, were calculated to identify dominant signaling sources and targets within the tumor microenvironment. Key ligand-receptor interactions mediating macrophage-tumor crosstalk were visualized using chord diagrams and hierarchy plots

Cell culture and siRNA knockdown

Human OC cell lines A2780 and SK-OV-3 were obtained from the American Type Culture Collection (ATCC) and cultured in RPMI-1640 medium supplemented with 10 % fetal bovine serum (FBS), 100 U/mL penicillin, and 100 μg/mL streptomycin at 37 °C in 5 % CO_2. STAB1-targeted small interfering RNA (si-STAB1) and non-targeting control

siRNA (si-NC) were synthesized by GenePharma (Shanghai, China) and transfected using Lipofectamine 3000 (Invitrogen) according to the manufacturer's protocol (final concentration: 50 nM). Knockdown efficiency was confirmed 48 h post-transfection.

RT-qPCR and Western blot analysis

Total RNA was extracted using TRIzol reagent (Invitrogen), and cDNA was synthesized with the PrimeScript RT Reagent Kit (Takara). Quantitative PCR was performed on a QuantStudio 5 system (Applied Biosystems) using SYBR Green Master Mix (Takara) with GAPDH as the internal control. Primer sequences for STAB1 were: forward 5′-GCTGAAGGTGCTGAAGGTGA-3′, reverse 5′-CAGCTTCTC-CAGCTTCTTGG-3′ Relative expression was calculated via the 2^{-ΔΔCt} method. For Western blotting, cells were lysed in RIPA buffer with protease inhibitors. Proteins (30 μg) were separated by 10 % SDS-PAGE, transferred to PVDF membranes, and probed with anti-STAB1 (1:1000, Abcam) and anti-GAPDH (1:5000, Abcam) antibodies overnight at 4 °C. Bands were visualized using ECL substrate (Thermo Fisher) and quantified with ImageJ software.

Functional assays

Cell proliferation was assessed using the Cell Counting Kit-8 (CCK-8; Dojindo) assay at 0, 24, 48, and 72 h post-transfection (absorbance at 450 nm). Colony formation was evaluated by seeding 500 cells/well in 6-well plates for 14 days, followed by crystal violet staining and colony counting. Migration was measured via Transwell assays (8-μm pores, Corning) with 10 % FBS as chemoattractant (24 h incubation, crystal violet staining) and wound healing assays (scratch created with 200-μL pipette tip, imaged at 0 and 48 h). All assays were performed in triplicate.

Statistical analysis

All analyses were conducted in R (version 4.3.0) or GraphPad Prism (version 9.0). Continuous data are presented as mean ± standard deviation. Differences were assessed by Student's *t*-test (two groups) or ANOVA (multiple groups), with $P < 0.05$ considered significant (*$P < 0.05$, **$P < 0.01$, ***$P < 0.001$).

Results

Identification of robust prognostic targets in ovarian cancer via multi-cohort transcriptomic screening

To identify differentially expressed genes (DEGs) associated with ovarian cancer (OC), we analyzed three independent Gene Expression Omnibus (GEO) datasets: GSE65857 (32 OC tumors vs. 32 normal tissues), GSE18520 (53 OC samples vs. 10 normal epithelia), and GSE14407 (12 OC epithelia vs. 12 normal). Volcano plots revealed distinct dysregulation patterns, with DEGs defined by $|\log_2(\text{fold change})| > 1$ and adjusted $P < 0.05$ (Fig. 1A): 5728 DEGs in GSE65857 (2969 up, 2759 down), 4226 in GSE18520 (2226 up, 2000 down), and 3297 in GSE14407 (1797 up, 1500 down). Venn diagrams identified 933 commonly upregulated and 106 downregulated DEGs (Fig. 1B). Hierarchical clustering of the top 25 DEGs demonstrated distinct expression profiles between tumor and normal tissues (Fig. 1C).

To translate these transcriptomic signatures into clinical relevance, we evaluated the prognostic value of candidate genes in the TCGA-OV cohort. Kaplan-Meier survival analysis identified that high expression of 15 candidate genes, including STAB1, SPP1, TEAD4, CNNM4, and SLC1A3, was significantly associated with poor Overall Survival (OS) (all $P < 0.05$, Fig. 2).

Prognostic significance of candidate genes

We investigated the survival significance of epithelial ovarian cancer (EOC)-derived differentially expressed genes (DEGs) in The Cancer Genome Atlas Ovarian Cancer (TCGA OV) dataset. Kaplan-Meier survival analysis was performed to evaluate the prognostic impact of gene expression levels on patient outcomes. Patients were stratified into high- and low-expression groups based on median expression values, and overall survival (OS) curves were generated for each gene. Differences

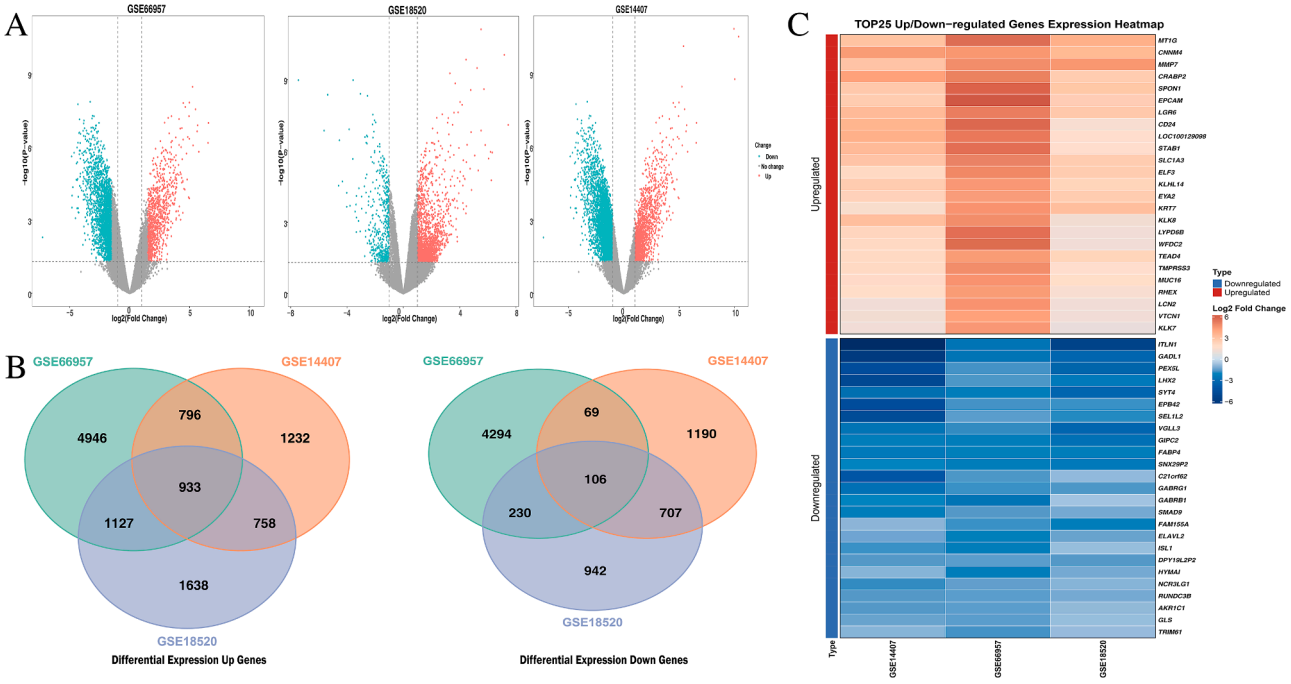

Fig. 1. Identification of DEGs in OC. (A) Volcano plots showing DEGs in GSE65857, GSE18520, and GSE14407 ($|\log_2(FC)| > 1$, adj. $P < 0.05$). (B) Venn diagrams of common upregulated and downregulated DEGs across datasets. (C) Heatmap of top 25 up- and downregulated DEGs with clustering.

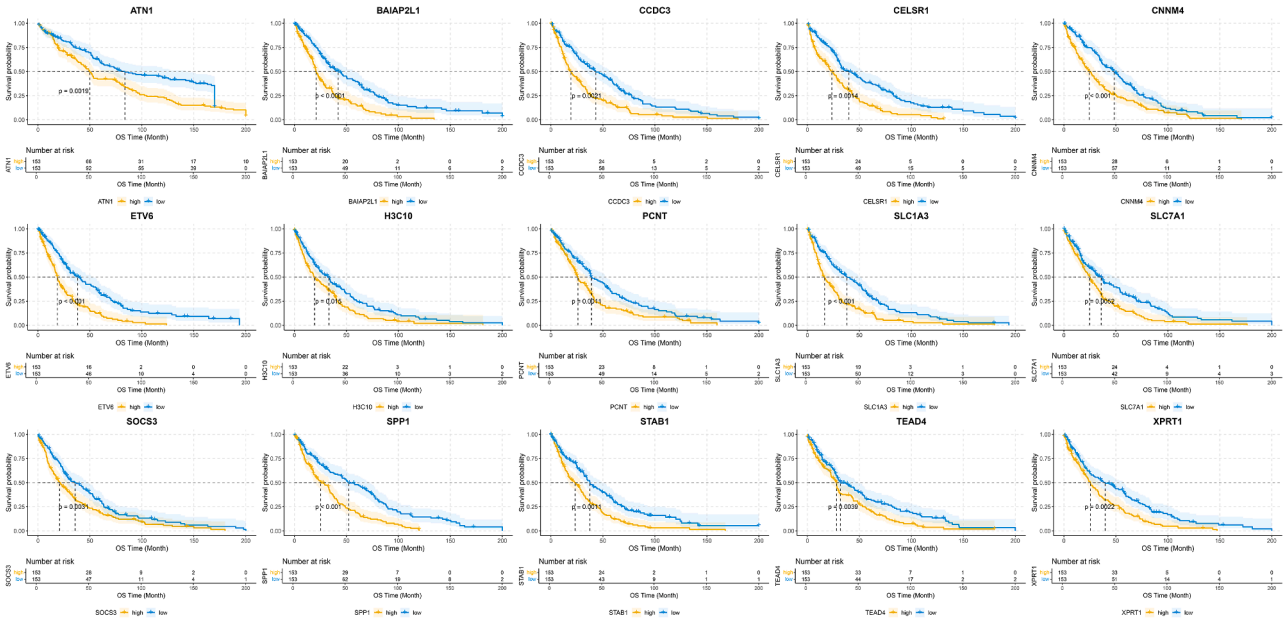

Fig. 2. Kaplan-Meier survival curves for candidate genes in TCGA-OV. High vs. low expression groups for genes like ATN1, BAIAP2L1, CDCA3, etc., with log-rank P-values ($P < 0.05$ indicating poor OS for high expression).

were assessed using the log-rank test, with $P < 0.05$ indicating significance.

High expression of ATN1 ($P = 0.015$), BAIAP2L1 ($P = 0.001$), CDCA3 ($P = 0.014$), CELSR1 ($P = 0.008$), CNNM4 ($P = 0.030$), ETV6 ($P = 0.014$), H3C10 ($P = 0.001$), PCNT ($P = 0.007$), SLC1A3 ($P = 0.038$), SLC7A1 ($P = 0.002$), SOCS3 ($P = 0.009$), SPP1 ($P = 0.001$), STAB1 ($P = 0.001$), TEAD4 ($P = 0.008$), and XPR1 ($P = 0.022$) was associated with poorer OS (Fig. 3). Patients with high expression exhibited significantly worse survival compared to those with low expression, highlighting these genes as potential prognostic biomarkers for risk stratification and treatment guidance in OC.

Feature selection for prognostic modeling

Feature selection for the prognostic model was performed using two methods, LASSO regression and SVM-RFE, to identify the most relevant biomarkers. LASSO regression identified the most significant predictors by tracing the coefficients of each feature across a range of regularization parameters (λ). As λ decreased, the degrees of freedom for the features increased, allowing for a more flexible fit. Through cross-

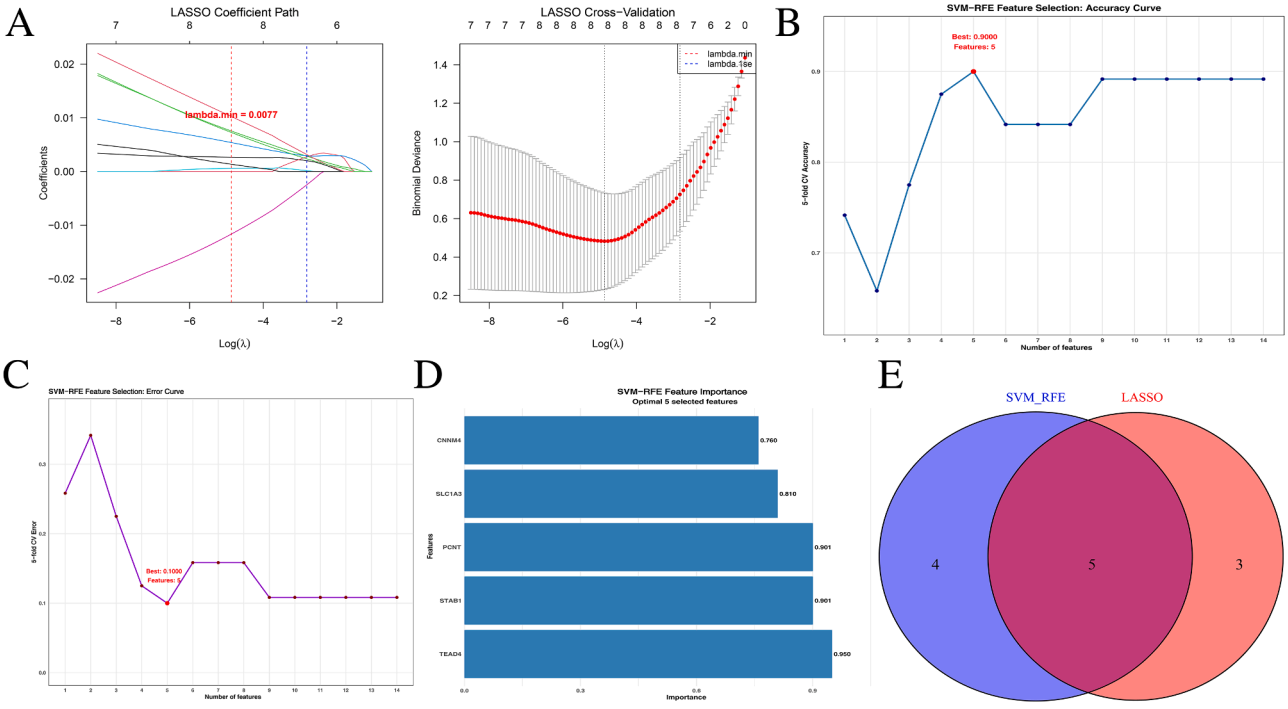

Fig. 3. Feature selection for prognostic modeling. (A) LASSO regression coefficient paths and cross-validation (optimal λ = 0.0077). (B) SVM-RFE error rate curve. (C) SVM-RFE accuracy curve (peak at 5 features). (D) Feature importance scores (top: CNNM4, SLC1A3, PCNT, STAB1, TEAD4). (E) Venn diagram of overlapping features from LASSO and SVM-RFE.

validation, the optimal λ value was determined to be λ_min = 0.0077, at which the model's binomial deviance was minimized to **0.4**, ensuring a robust model fit, as depicted in Fig. 3A. he SVM-RFE (Support Vector Machine Recursive Feature Elimination) method was subsequently applied to iteratively eliminate less informative features, thereby reducing the feature set. The model achieved its highest accuracy of 0.900 when 5 features were retained, with an associated error rate of 0.100, as illustrated in Fig. 3B-C. The intersection of these two algorithms pinpointed five core genes: CNNM4, SLC1A3, PCNT, STAB1, and TEAD4, ranked by their feature importance (Fig. 3D-E). Among them, STAB1 ranked highly and was selected for further investigation due to its known potential roles in immune regulation.

Construction and validation of the STAB1-inclusive prognostic model

Univariate Cox regression identified CNNM4 (HR = 0.71, 95 % CI 0.55–0.92, P = 0.009), SLC1A3 (HR = 1.41, 95 % CI 1.10–1.80, P = 0.007), PCNT (HR = 1.25, 95 % CI 1.05–1.49, P = 0.012), STAB1 (HR = 1.25, 95 % CI 1.05–1.49, P = 0.012), and TEAD4 (HR = 1.25, 95 % CI 1.05–1.49, P = 0.012) as significant (Fig. 4B). Multivariate analysis confirmed independence (CNNM4 protective, others risk-associated) (Fig. 4A). The nomogram integrated expression scores for 1-, 3-, and 5-year OS prediction (Fig. 4C), with calibration showing strong alignment (Hosmer-Lemeshow ρ = 0.832, 1000 bootstraps) (Fig. 4D). ROC in validation datasets yielded AUCs of 0.772 (GSE14407), 0.915 (GSE65857), 0.802 (GSE18520), and 0.674 (GSE38666) (Fig. 4E). Among the signature genes, STAB1 showed high feature importance and known links to immune modulation, warranting further exploration of its role in the tumor microenvironment.

Single-cell Atlas redefines the cellular localization of STAB1 in the TME

While bulk RNA-seq established STAB1 as a prognostic marker, its cellular source remained ambiguous. We utilized GSE184880 single-cell RNA sequencing (scRNA-seq) to map the landscape of the OC tumor microenvironment (TME). Unsupervised Seurat clustering initially identified 28 distinct cell clusters (Fig. 5A). To accurately characterize these populations, we evaluated the expression profiles of the top marker genes across all clusters (Fig. 5B) and validated them against canonical lineage markers (Fig. 5C). This comprehensive approach enabled the precise annotation and spatial visualization of major cell types—including Epithelial cells, Fibroblasts, Endothelial cells, Macrophages, and T cells—within the UMAP embedding (Fig. 5D). Contrary to the traditional view of STAB1 as solely a tumor cell marker, FeaturePlot and Violin plot analyses revealed that STAB1 is predominantly enriched in the Macrophage and Endothelial compartments (Fig. 5E-F), with heterogeneous expression observed in Epithelial cells. This "dual-compartment" distribution suggests STAB1 functions as a bridge between the stromal microenvironment and tumor cells.

STAB1 defines a pro-tumorigenic, perivascular-like M2 macrophage subpopulation

To dissect the role of STAB1 in the immune microenvironment, we re-clustered the macrophage population into seven subsets (Fig. 6A). Quantitative analysis revealed a significant expansion of CD163+ and LYVE1+ macrophage subsets in tumor tissues compared to normal tissues (Fig. 6B). Notably, STAB1 expression was specific to the LYVE1+ and CD163+ subpopulations (Fig. 6C). LYVE1+ macrophages are characteristically known as perivascular tumor-associated macrophages (TAMs). Correlation analysis at the single-cell level provided definitive evidence of polarization: STAB1 was strongly positively correlated with M2 markers CD163 (R = 0.42) and MRC1 (R = 0.34) (Fig. 6D-F), but showed no correlation with the anti-tumor M1 phenotype (Fig. 6G).

STAB1 marks a hyper-aggressive tumor subpopulation with EMT and stemness features

We investigated the heterogeneity within the tumor (Epithelial) compartment. Sub-clustering revealed distinct tumor cell states (Fig. 7A). Although STAB1 expression in tumor cells is generally lower than in macrophages, Violin and Feature plot analyses demonstrated that it specifically marks a high-risk subpopulation (Fig. 7C-D) characterized by THY1 and MUC4 expression (Fig. 7B), known markers of stemness and metastasis. To further elucidate its role, we stratified epithelial cells into STAB1-high and STAB1-low groups (Fig. 7F). Differential expression analysis between these groups revealed a profound transcriptomic shift (Fig. 7E). Most importantly, STAB1-high tumor cells exhibited a distinct Epithelial-Mesenchymal Transition (EMT) and stemness signature, characterized by the concurrent upregulation of

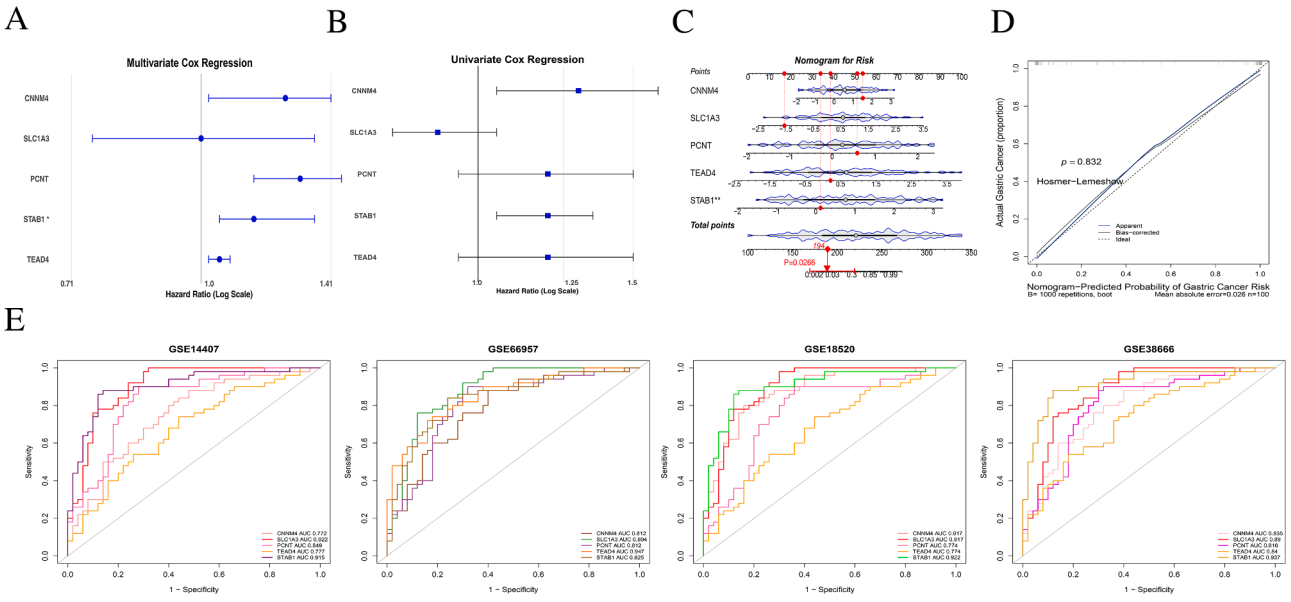

Fig. 4. Construction and validation of prognostic signature. (A) Multivariate Cox regression forest plot (HRs for five genes). (B) Univariate Cox regression forest plot. (C) Nomogram integrating genes for 1-, 3-, 5-year OS prediction. (D) Calibration plots with bootstrap validation (Hosmer-Lemeshow P = 0.832). (E) ROC curves in validation datasets (AUC: 0.772–0.915).

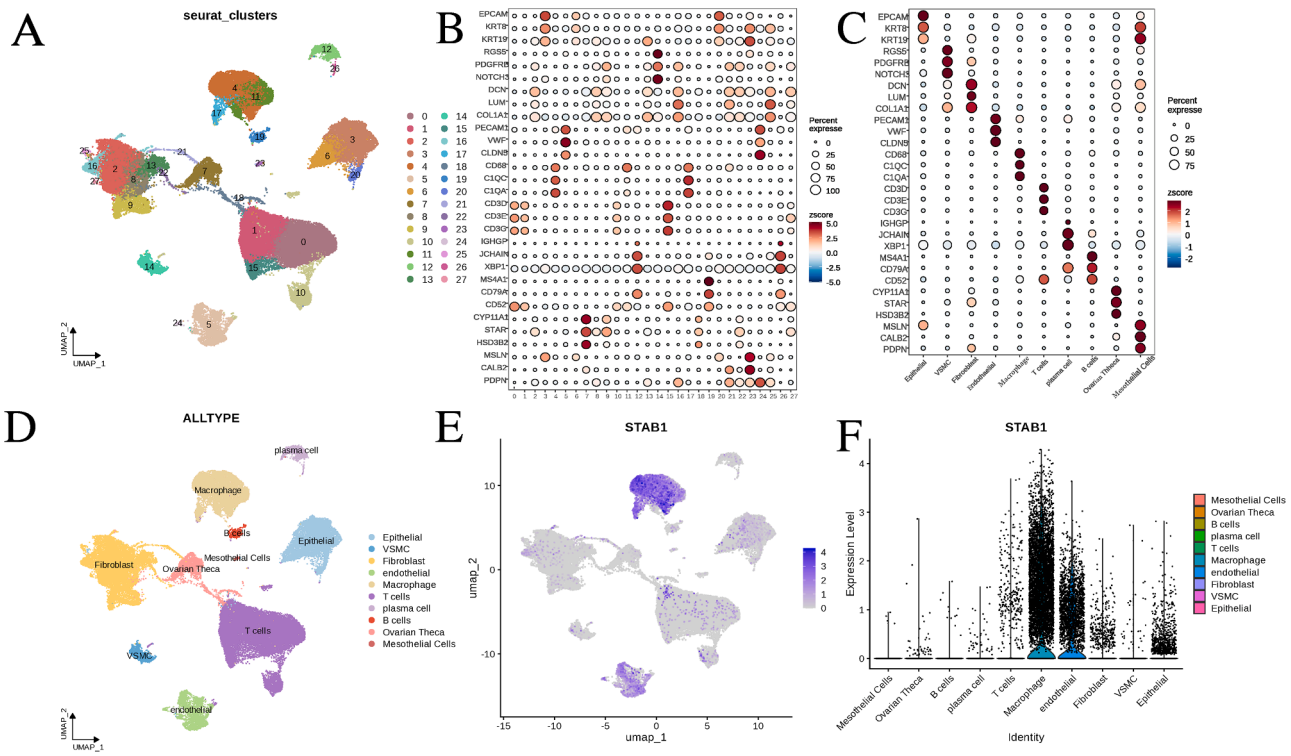

Fig. 5. Global Cellular Landscape and *STAB1* Expression Patterns. (A) UMAP visualization of 28 distinct cell clusters identified by Seurat clustering. (B) Dot plot displaying the expression of top marker genes across the identified cell clusters. (C) Dot plot showing canonical marker genes used to identify major cell types, including epithelial cells, fibroblasts, endothelial cells, macrophages, and T cells. (D) UMAP plot showing the distribution of annotated major cell types. (E) Feature plot illustrating the distribution of *STAB1* gene expression across the cellular landscape. (F) Violin plot quantifying *STAB1* expression levels across different cell types, highlighting elevated expression in macrophages and endothelial cells.

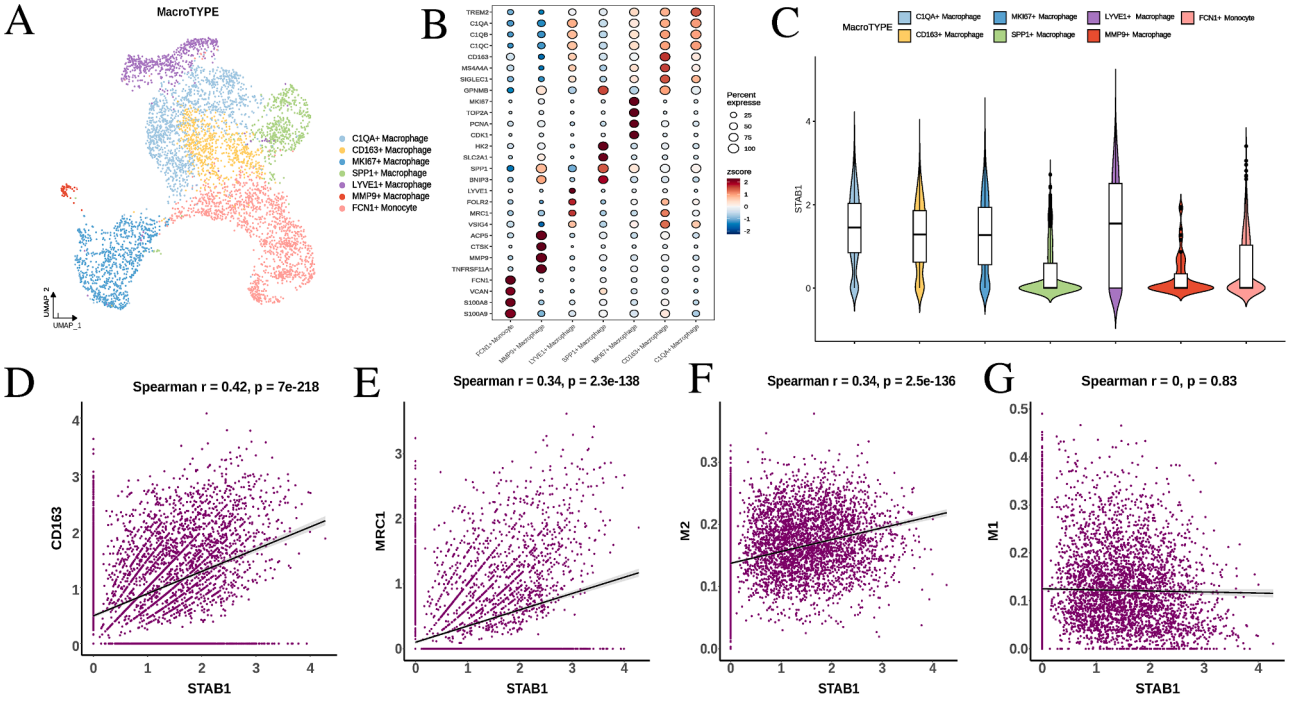

Fig. 6. Macrophage Subset Characterization and Correlation with STAB1. (A) UMAP visualization of macrophage subpopulations (MacroTYPE). (B) Dot plot illustrating specific marker genes for distinct macrophage subsets. (C) Violin plot showing differential expression of STAB1 across macrophage subsets, with higher levels observed in C1QA+ and CD163+ clusters. (D–E) Scatter plots demonstrating a positive correlation between STAB1 expression and M2 macrophage markers CD163 (Spearman $r = 0.42$, D) and MRC1 (Spearman $r = 0.34$, E). (F–G) Correlation analysis revealing a positive association between STAB1 and M2 polarization scores (F), while no significant correlation was observed with M1 polarization scores (G).

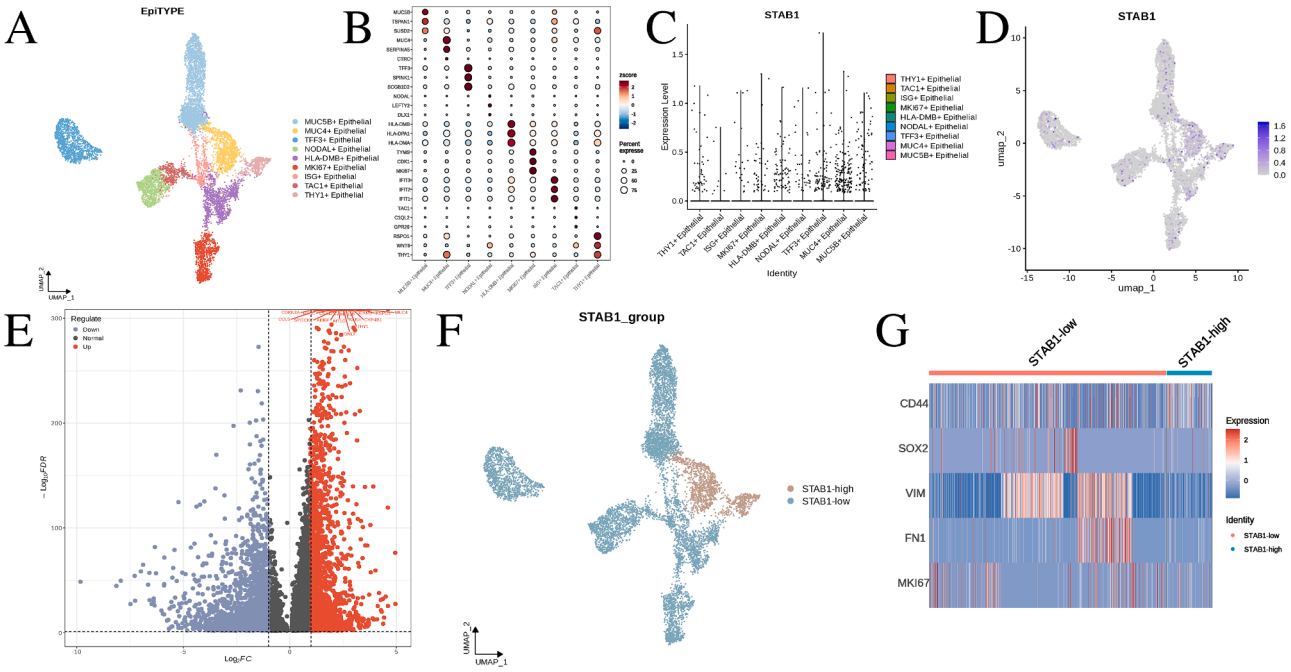

Fig. 7. Epithelial Heterogeneity and STAB1-Mediated Phenotypic Shifts. (A) UMAP visualization of epithelial cell subpopulations (EpiTYPE). (B) Dot plot displaying the expression of signature genes for different epithelial subsets. (C) Violin plot and (D) Feature plot illustrating the expression distribution of STAB1 within epithelial subpopulations. (E) Volcano plot showing differentially expressed genes (DEGs) between STAB1-high and STAB1-low groups. (F) UMAP plot of epithelial cells stratified by STAB1 expression levels (High vs. Low). (G) Heatmap indicating significant upregulation of EMT-related genes (CD44, SOX2, VIM, FN1) and the proliferation marker MKI67 in the STAB1-high group.

CD44, Vimentin (VIM), and Fibronectin (FN1) (Fig. 7G). This suggests potential involvement of STAB1 in defining the 'metastatic seeds' within the tumor bulk.

Intercellular communication networks and macrophage functional in the TME

CellChat analysis of intercellular communication revealed distinct network topologies between normal and tumor tissues. The tumor ecosystem demonstrated intensified signaling connectivity with elevated aggregated interaction weights, characterized by robust macrophage-epithelial interactions (Fig. 8A). Network centrality analysis highlighted a clear hierarchical shift in cellular roles (Fig. 8B). In normal tissue, fibroblasts functioned as the primary signaling sources. In contrast, macrophages in the tumor microenvironment transitioned into dominant signaling hubs with high outgoing interaction strength, while epithelial and T cells served as the primary downstream targets, exhibiting high incoming interaction strengths.

Experimental validation: STAB1 is essential for tumor proliferation and metastasis

To assess the functional role of STAB1 in ovarian cancer, we performed in vitro loss-of-function assays. We successfully knocked down STAB1 in two ovarian cancer cell lines, A2780 and SK-OV-3, using siRNA, confirmed by Western Blot and qPCR (Fig. 9A-B). Consistent with our single-cell EMT findings, STAB1 silencing significantly inhibited cell proliferation in CCK-8 assays (Fig. 9C) and suppressed long-term growth in colony formation assays (Fig. 9F). Furthermore, Transwell and wound healing assays demonstrated that STAB1 knockdown markedly impaired the migration and invasion capabilities of both OC cell lines (Fig. 9D-E). These results experimentally confirm that targeting STAB1 disrupts the intrinsic malignant behaviors of ovarian cancer cells.

Discussion

Ovarian cancer (OC) remains the most lethal gynecologic malignancy, characterized by high heterogeneity and a propensity for peritoneal dissemination [1,12]. Despite recent advances in cytoreductive surgery and the introduction of PARP inhibitors, the recurrence rate remains alarmingly high due to therapeutic resistance [2,13]. Consequently, there is an urgent need to identify robust biomarkers that can guide precise risk stratification and reveal novel therapeutic targets. In this study, we integrated multi-cohort transcriptomic screening with machine learning to identify a robust 5-gene prognostic signature (CNNM4, SLC1A3, PCNT, STAB1, TEAD4). Among these, our results highlight STAB1 as a pivotal dual-compartment regulator that orchestrates a pro-tumorigenic ecosystem through both immune suppression and intrinsic tumor plasticity.

The identified prognostic genes have been partially implicated in cancer biology, reinforcing the validity of our model. For instance, TEAD4 acts as a central regulator of the Hippo pathway, promoting metastasis in various cancers [14], while SLC1A3 supports the metabolic adaptation of cancer cells by regulating glutamate availability, a crucial nutrient for tumor survival [15]. However, the role of STAB1 in OC has been less defined. Biologically, STAB1 is a scavenger receptor involved in tissue homeostasis and the clearance of "self" antigens [9,16]. Our study expands this understanding by demonstrating that high STAB1 expression is a determinant of poor overall survival in OC. This aligns with recent findings that scavenger receptors are not merely waste handlers but active participants in immune regulation [9,12].

A major finding of our single-cell analysis is the specific enrichment of STAB1 in M2-like tumor-associated macrophages (TAMs), particularly the LYVE1+/CD163+ subset. TAMs are key regulators of tumor immunity, often hampering the efficacy of T-cell-based therapies [17, 18]. Our data correlates STAB1 with an immunosuppressive phenotype, consistent with the observation that distinct interstitial macrophage populations occupy specific niches to support tissue pathology [19]. Furthermore, metabolic reprogramming is a hallmark of TAMs [20], and

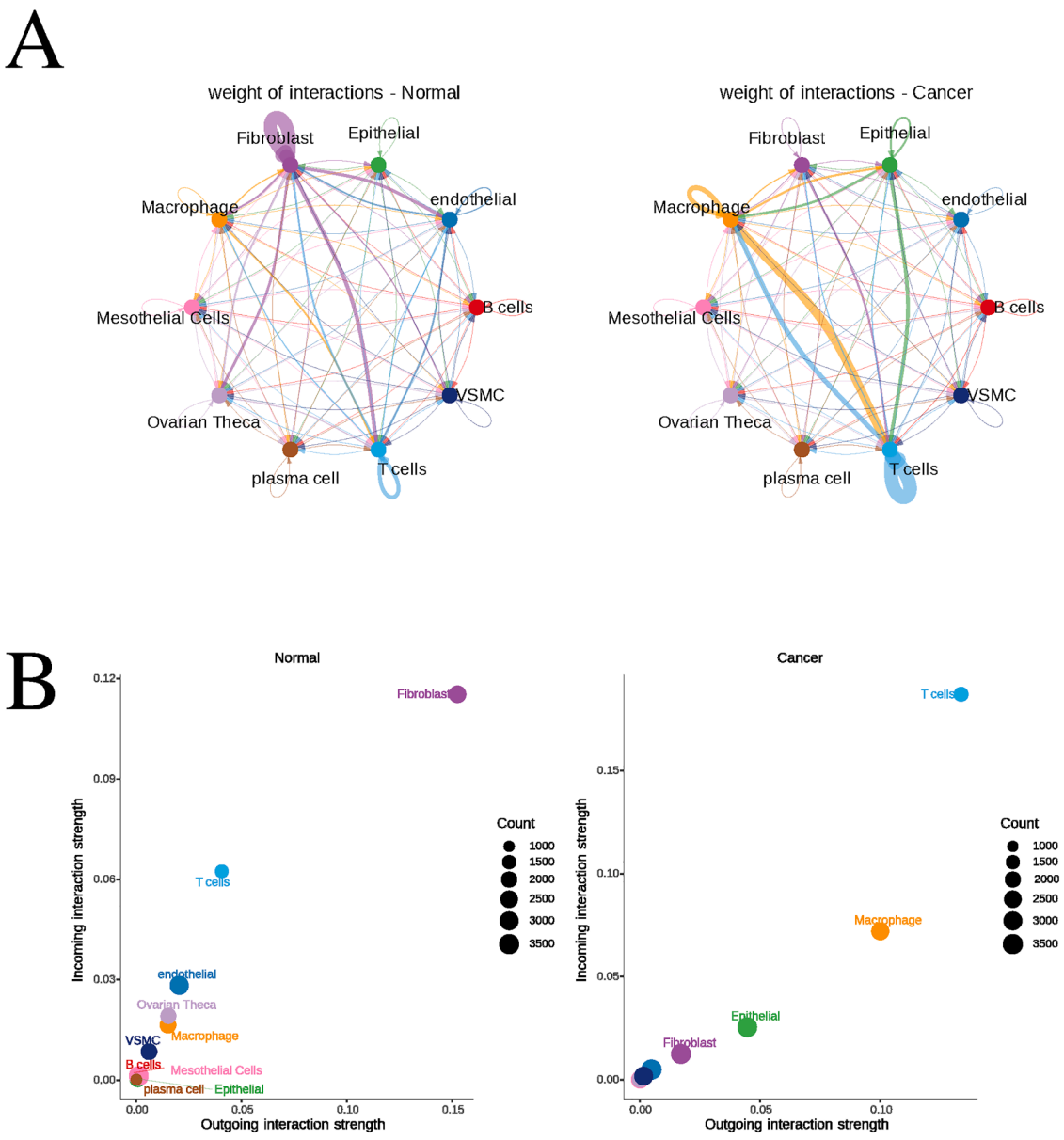

Fig. 8. Intercellular Communication Networks and Functional Shifts in the TME (A) Circle plots illustrating intercellular communication networks in Normal (left) and Cancer (right) tissues using CellChat analysis. Line thickness represents the aggregated interaction weight, revealing a denser and more intensified signaling network in the tumor microenvironment. (B) Scatter plots depicting dominant signaling sources and targets based on network centrality measures.

STAB1 may facilitate this by scavenging extracellular ligands that sustain an anti-inflammatory milieu [9]. Notably, the STAB1+ macrophages in our study resemble the "onco-fetal" reprogrammed macrophages described by Sharma et al. [21], which drive immunosuppression in the tumor microenvironment (TME). This suggests that STAB1 is a functional marker of a deeply immunosuppressive myeloid state, making it a potential target for repolarization therapies. Indeed, antibodies targeting CLEVER-1 (STAB1) have been shown to mobilize anti-tumor immunity by disabling the M2 phenotype [22] and controlling metastasis [23], validating our finding that STAB1 represents a high-priority "myeloid target" as discussed by Zhang et al. [24].

Beyond the immune compartment, our study unveils a novel, intrinsic role for STAB1 in epithelial tumor cells. Contrary to its classical restriction to scavenger cells, we identified a high-risk STAB1+ tumor subpopulation characterized by EMT features and stemness markers like THY1 and CD44. Zhang et al. [25] previously identified a THY1+ cancer stem cell-like subpopulation in OC with high plasticity, and our results suggest STAB1 marks this precise "metastatic seed." The co-expression of CD44 is particularly significant, as CD44 is a master regulator of tumorigenesis and therapy resistance [26], often functioning through interactions with ligands like Osteopontin (SPP1) to promote migration [11]. We hypothesize that STAB1 may cooperate with these pathways, potentially modulating PI3K/AKT signaling, a critical regulator of EMT to drive invasion [27]. Our in vitro results, showing that STAB1 knockdown impairs migration and proliferation, support the concept that tumor cell biodiversity drives microenvironmental reprogramming [28], where aggressive subclones dictate the behavior of the surrounding stroma.

The intercellular communication analysis (CellChat) further places STAB1 at the center of a complex interaction network. We observed intensified signaling between macrophages and tumor cells, a phenomenon echoed by Armingol et al. [29] as a hallmark of tissue dysfunction. Specifically, the interaction patterns we observed resemble the crosstalk between SPP1+ macrophages and FAP+ fibroblasts seen in colorectal cancer [10], suggesting a conserved mechanism of stromal support across solid tumors. This crosstalk likely creates a physical and

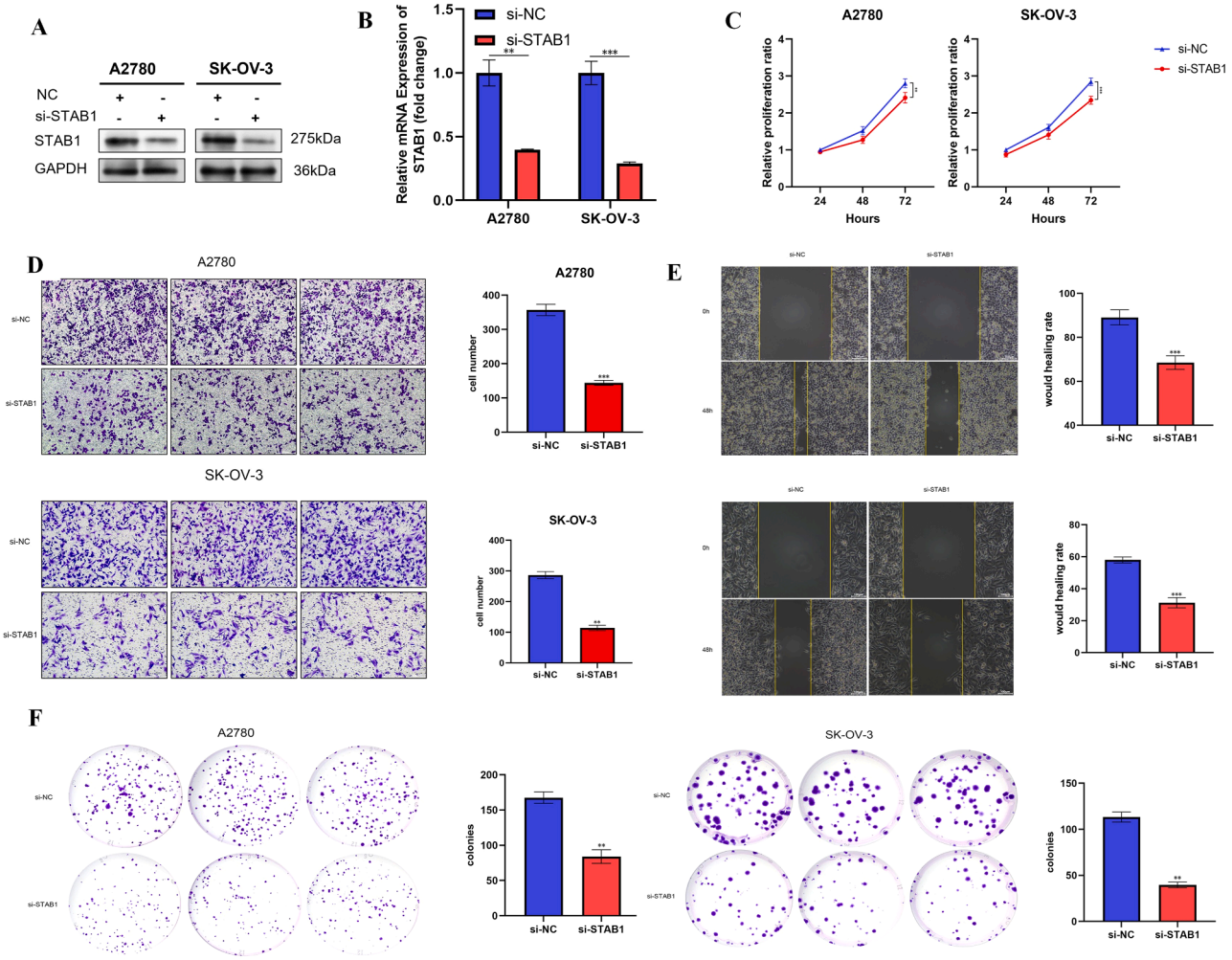

Fig. 9. (A). Western blot, (B). qPCR, (C). Proliferation, (D). Transwell, (E). wound healing, (F). Colony formation of SK-OV-3 and A2780 cell lines transfected with si-STAB1 and si-NC plasmids. $P < 0.05$, ** for $P < 0.01$, and *** for $P < 0.001$.

chemical barrier that excludes effector T cells, contributing to the "cold" tumor phenotype typical of OC [30]. Rao et al. [31] emphasized the importance of tissue architecture in spatial transcriptomics. Although our study was based on scRNA-seq and therefore lacks direct spatial resolution, the perivascular-like LYVE1⁺ signature of STAB1⁺ macrophages suggest a spatially restricted niche that may facilitate hematogenous dissemination. Consistent with this, our single-cell analyses indicate an enrichment of STAB1 within LYVE1⁺ perivascular-like TAMs in ovarian cancer. While STAB1 has been primarily associated with scavenging-related functions, its relationship to EMT and stemness programs in highly aggressive ovarian cancer subpopulations has not been well defined; our data extend existing observations by supporting a potential link between STAB1-associated macrophage states and these malignant phenotypes.

Clinically, these findings have profound implications for immunotherapy. Current checkpoint inhibitors have shown limited success in OC [32]. The STAB1-mediated immunosuppression offers a mechanistic explanation for this resistance. Targeting STAB1 could offer a "two-pronged" therapeutic strategy: (1) reversing the M2 macrophage blockade [22,17,18] and (2) directly inhibiting the invasive capacity of stem-like tumor cells [11,25]. Furthermore, our prognostic nomogram provides a robust tool for clinical utility. Future studies should focus on validating these mechanisms in patient-derived organoids [33], which better recapitulate the TME than 2D cultures, and exploring the potential of STAB1 inhibitors in combination with standard chemotherapy [28].

Limitations

Despite these promising results, our study has limitations. First, while we validated the prognostic model in multiple cohorts, the retrospective nature of the data requires prospective validation. Second, although we confirmed the functional phenotype of STAB1 in vitro, the precise molecular signaling pathways downstream of STAB1 in tumor cells remain to be fully elucidated. A2780 and SK-OV-3, while practical for initial in vitro screens, do not accurately represent the genomic complexity of High-Grade Serous Ovarian Cancer. Future studies using in vivo orthotopic models are needed to evaluate the efficacy of STAB1 inhibitors in curbing peritoneal metastasis.

Conclusion

In conclusion, we identified a robust transcriptomic signature for ovarian cancer prognosis and unraveled the multifaceted role of STAB1. We demonstrate that STAB1 serves as a nexus between the immunosuppressive microenvironment and tumor cell intrinsic plasticity. These findings suggest that STAB1 is a promising dual-compartment therapeutic target capable of disrupting the symbiotic pro-tumorigenic interaction between cancer cells and TAMs.

Data availability

The GEO datasets (https://www.ncbi.nlm.nih.gov/gene). The TCGA-

OV cohort was downloaded from the TCGA portal (https://portal.gdc.cancer.gov/), and genetic data of OV was accessed from cBioPortal (http://www.cbioportal.org/).

Funding

This study was supported by 2024 High-quality Development Research Project of Shenzhen Bao'an Public Hospital (Grant No BAGZL2024199) and National Health Commission Medical and Health Science and Technology Development Research Center Project (Grant No WKZX2024DN0149).

CRediT authorship contribution statement

Yuqiang Zhang: Writing – review & editing, Writing – original draft. **Juan Chen:** Writing – review & editing, Writing – original draft, Methodology. **Li Tang:** Methodology, Data curation. **Xiaohai Sun:** Methodology, Investigation. **Ling Yang:** Writing – review & editing, Writing – original draft. **Zhaomei Zhong:** Writing – review & editing, Writing – original draft, Resources.

Declaration of competing interest

There is no conflict of interest.

References

[1] S. Lheureux, C. Gourley, I. Vergote, G. Kristensen, Epithelial ovarian cancer, Lancet 393 (2019) 1240–1253, https://doi.org/10.1016/S0140-6736(18)32552-2.
[2] R.L. Siegel, A.N. Giaquinto, A. Jemal, Cancer statistics, 2024, CA *Cancer J. Clin.* 74 (2024) 12–49, https://doi.org/10.3322/caac.21820.
[3] D.C. Hinshaw, L.A. Shevde, The tumor microenvironment innately modulates cancer progression, Cancer Res. 79 (2019) 4557–4566, https://doi.org/10.1158/0008-5472.CAN-18-3962.
[4] N. Cheng, et al., Targeting tumor-associated macrophages as a new therapeutic strategy for malignancy, Signal Transduct. Target. Ther. 9 (2024) 10, https://doi.org/10.1038/s41392-023-01703-w.
[5] A. Mantovani, F. Marchesi, A. Malesci, L. Laghi, P. Allavena, Tumour-associated macrophages as treatment targets in oncology, Nat. Rev. Clin. Oncol. 14 (2017) 399–416, https://doi.org/10.1038/nrclinonc.2016.217.
[6] M.L. Suvà, I. Tirosh, Single-cell RNA sequencing in cancer: lessons learned and emerging challenges, Mol. Cell 75 (2019) 7–35, https://doi.org/10.1016/j.molcel.2019.05.003.
[7] B. Izar, et al., A single-cell landscape of high-grade serous ovarian cancer, Nat. Med. 26 (2020) 1272–1280, https://doi.org/10.1038/s41591-020-0926-0.
[8] Y. You, et al., Artificial intelligence in cancer target identification and drug discovery, Signal Transduct. Target. Ther. 7 (2022) 156, https://doi.org/10.1038/s41392-022-01008-z.
[9] J. Kzhyshkowska, et al., Stabilin-1, a scavenger receptor with multiple functions in tissue homeostasis and pathology, Immunobiology 215 (2010) 766–777, https://doi.org/10.1016/j.imbio.2010.05.018.
[10] J. Qi, et al., Single-cell and spatial analysis reveal interaction of FAP+ fibroblasts and SPP1+ macrophages in colorectal cancer, Nat. Commun. 13 (2022) 1742, https://doi.org/10.1038/s41467-022-29366-6.
[11] J. Wei, et al., Osteopontin mediates intracellular signaling to promote the migration and invasion of osteosarcoma cells, Oncol. Rep. 41 (2019) 2289–2298, https://doi.org/10.3892/or.2019.7038.
[12] U.A. Matulonis, et al., Ovarian cancer, Nat. Rev. Dis. Primers 2 (2016) 16061, https://doi.org/10.1038/nrdp.2016.61.
[13] A.J. Cortez, P. Tudrej, K.A. Kujawa, K.M. Lisowska, Advances in ovarian cancer therapy, Cancer Chemother. Pharmacol. 81 (2018) 17–38, https://doi.org/10.1007/s00280-017-3501-8.
[14] H.D. Huh, et al., TEAD4 acts as a central regulator of the Hippo pathway to promote cancer metastasis, Exp. Mol. Med. 51 (2019) 1–12, https://doi.org/10.1038/s12276-019-0247-3.
[15] M. Tajan, K.H. Vousden, Dietary glutamate and cancer, Nat. Metab. 2 (2020) 759–760, https://doi.org/10.1038/s42255-020-0259-x.
[16] J. Canton, D. Neculai, S. Grinstein, Scavenger receptors in homeostasis and immunity, Nat. Rev. Immunol. 13 (2013) 621–634, https://doi.org/10.1038/nri3515.
[17] D.G. DeNardo, B. Ruffell, Macrophages as regulators of tumour immunity and immunotherapy, Nat. Rev. Immunol. 19 (2019) 369–384, https://doi.org/10.1038/s41577-019-0127-6.
[18] M.J. Pittet, et al., Clinical relevance of tumour-associated macrophages, Nat. Rev. Clin. Oncol. 19 (2022) 402–421, https://doi.org/10.1038/s41571-022-00620-6.
[19] S. Chakarov, et al., Two distinct interstitial macrophage populations coexist across tissues in specific subtissular niches, Science 363 (2019) eaau0964, https://doi.org/10.1126/science.aau0964.
[20] I. Vitale, et al., Macrophages and metabolism in the tumor microenvironment, Cell Metab. 30 (2019) 36–50, https://doi.org/10.1016/j.cmet.2019.06.001.
[21] A. Sharma, et al., Onco-fetal reprogramming of endothelial cells drives immunosuppressive macrophages in hepatocellular carcinoma, Cell 183 (2020) 377–394, https://doi.org/10.1016/j.cell.2020.08.040.
[22] M. Hollmén, et al., Antibodies targeting CLEVER-1 mobilize antitumor immunity and disable M2 macrophage immunosuppression, Clin. Cancer Res. 26 (2020) 3863–3874, https://doi.org/10.1158/1078-0432.CCR-19-3392.
[23] M. Viitala, et al., Clever-1/Stabilin-1 controls cancer growth and metastasis, Clin. Cancer Res. 20 (2014) 6452–6464, https://doi.org/10.1158/1078-0432.CCR-14-1236.
[24] L. Zhang, et al., Single-cell analyses inform mechanisms of myeloid-targeted therapies in colon cancer, Cell 181 (2020) 442–459, https://doi.org/10.1016/j.cell.2020.03.048.
[25] X. Zhang, et al., Identification of a THY1+ cancer stem cell-like subpopulation with high plasticity in ovarian cancer, Clin. Cancer Res. 25 (2019) 634–645, https://doi.org/10.1158/1078-0432.CCR-18-2345.
[26] C. Chen, et al., The roles of CD44 in tumorigenesis and cancer therapy, Cell Death Dis. 9 (2018) 867, https://doi.org/10.1038/s41419-018-1071-7.
[27] R. Rashed, et al., PI3K/AKT signaling pathway as a critical regulator of epithelial-mesenchymal transition in colorectal cancer, Cell Commun. Signal. 21 (2023) 198, https://doi.org/10.1186/s12964-023-01215-2.
[28] L. Ma, et al., Tumor cell biodiversity drives microenvironmental reprogramming in liver cancer, Cancer Cell 36 (2019) 418–430, https://doi.org/10.1016/j.ccell.2019.08.007.
[29] E. Armingol, et al., Deciphering cell–cell interactions and communication from gene expression, Nat. Rev. Genet. 22 (2021) 71–88, https://doi.org/10.1038/s41576-020-00292-x.
[30] M. Hornburg, et al., Single-cell dissection of cellular components and interactions shaping the tumor immune phenotypes in ovarian cancer, Cancer Cell 39 (2021) 928–944, https://doi.org/10.1016/j.ccell.2021.04.004.
[31] A. Rao, et al., Exploring tissue architecture using spatial transcriptomics, Nature 596 (2021) 211–220, https://doi.org/10.1038/s41586-021-03634-9.
[32] K. Odunsi, Immunotherapy in ovarian cancer, Ann. Oncol. 28 (2017) viii1–viii7, https://doi.org/10.1093/annonc/mdx444.
[33] J. Drost, H. Clevers, Organoids in cancer research, Nat. Rev. Cancer 18 (2018) 407–418, https://doi.org/10.1038/s41568-018-0007-6.